# QUANTIFYING CRACK TIP DISPLACEMENT FIELDS: T-STRESS AND CTOA

**J. R. Yates, M. Zanganeh, D. Asquith and Y. H. Tai**

Dept of Mechanical Engineering, University of Sheffield, UK.

E-mail: j.yates@sheffield.ac.uk

***ABSTRACT***. *Crack paths under both fatigue and fracture conditions are governed by the crack tip displacement field and the material deformation characteristics, including those influenced by metallurgical anisotropy. Experimental techniques such as thermoelasticity and photoelasticity have been successfully used to characterise the elastic stress fields around cracks but they do not take into account either plasticity or anisotropy. Considerable work has been carried out to characterise crack tip stress fields from displacement measurements. The current method of choice for obtaining displacement field data is digital image correlation (DIC). This technique has recently been extended to determine T-stresses in cracked specimens. Full field displacement techniques also have the advantage that the influence of crack tip plasticity may be evaluated directly. This paper describes the technique for obtaining T-stresses from displacement fields measured using DIC. The algorithm used was based on Williams' solution to obtain both K and the non-singular term T. Results have shown that the technique works well when compared with finite element simulations. A significant amount of work was also carried out to characterise displacement fields around a crack during the steady state tearing under monotonic load. The fracture parameter of interest was the crack tip opening angle (CTOA). Results from displacement field characterisation corresponded well to more conventional techniques. It also showed clearly the effects of measurement length and position on CTOA data.*

## INTRODUCTION

The path that a crack follows, whether it is under cyclic or monotonic loading, is strongly influenced by the elastic and plastic displacement field at the crack tip. These

displacements are governed by a combination of material deformation behaviour, the mechanics of the loading and the geometry of the structure.

The material aspects that influence the crack path include the anisotropy of the microstructure; the size and spatial distributions of second phase particles; as well as the non-linear hardening response. The nature of the loading applied to the crack is important, both in term of multiaxiality and the state of internal or residual stresses. The interaction of these forces with the geometry of the structure is the third essential factor influencing the path of the crack. This is often manifest as a change in crack behaviour as the constraint changes from laboratory specimens to engineering structures.

For many years, our investigations into crack paths, has been based on characterising the crack path displacement field through the elastic component. Photoelastic stress analysis, thermoelaticity, caustics, Moire interferometry and many other have been used to successfully characterise the elastic stress fields around cracks but these techniques are not able to take into consideration effects of plasticity or anisotropy [1]. This has led to considerable work on developing techniques for characterising crack tip stress fields from displacement field measurements. The recent availability of high quality, high resolution digital cameras has enabled the full field elastic-plastic displacement field to be measured directly. This has opened up the possibility of exploring the influence of plastic deformations around the crack tip on the path of the growing crack.

The current method of choice for characterising displacement fields is digital image correlation (DIC) which is a relatively straight forward and cost effective technique. Previous work by Lopez-Crespo [2] has demonstrated that it is possible to experimentally characterise stress intensity factors accurately from displacement field measurements around the crack tip based on Muskhelishvili's formulations. Other workers have also done this successfully based on other analytical approaches [3, 4].

Further work has since been carried out to determine experimentally K and the T-stresses in cracked specimens using Williams' solution [5, 6]. This is a significant step forward because it allows the constraint levels around the crack tip to be quantified. Details of the technique and examples of results obtained will follow this section.

A significant amount of work has also been carried out to characterise displacement fields around a crack during the steady state tearing under monotonic load. The challenge in this situation is that the displacement field is not well characterised by either a conventional linear elastic term, such as $K_I$, or by a non-linear parameter such as $J_I$. Instead, the crack tip opening angle (CTOA) is considered to be a promising approach for characterising ductile fracture where there is significant crack extension [7]. There are various techniques for measuring CTOA [8]. The technique and results presented in this paper will be based on displacement field measurements.

The overall aim of this paper is to provide an overview of the work being done on displacement field based experimental and analytical techniques which can help with the better identification of parameters influencing crack paths.

## EXPERIMENTAL EVALUATION OF T-STRESS

Like geometric moiré, moiré interferometry, holographic interferometry, and electronic speckle pattern interferometry (ESPI), digital image correlation (DIC) is also a full field technique to measure in- and out- of plane displacement fields. DIC is based on the mathematical correlation of the change in light intensity patterns of sequential digital images captured from the surface of the specimen while it undergoes deformation. The grey scale pattern of the surface is compared before (reference image) and after (deformed image) applying the deformation to the specimen and hence the displacement vectors are determined. These experimental data are processed and fitted to appropriate mathematical descriptions of the crack displacement field to extract the crack characterising parameters. Since DIC uses pairs of digital images, the equipment needed is much simpler than that required for other optical techniques.

### *T-stress extraction from DIC data: methodology*

There are two different approaches to tackle any elasticity problem using experimental data. The first approach is to guess a general form of analytical function and fit this to the experimental data and then determine the displacement field and stress field. Muskhelishvili's [9] approach belongs to this group in which two complex analytical functions need to be used.

The second approach is to guess an analytical stress function, it can be complex or not, satisfying the boundary conditions and determining the displacement and stress field analytically. These analytical fields can be fitted to the experimental data and the required parameters, for example, T-stress and stress intensity factor, can be determined. One such analytical solution is Williams' asymptotic formulation [10].

In this work Williams' approach is used to extract the T-stress and SIF from experimental displacement data obtained from DIC measurements.

### *Williams' approach*

Based on Williams' approach the stress field ahead of a crack can be expressed as an infinite series. In a plane mixed mode I and II condition this stress field is expressed as equations (1) and (2).

$$\text{Mode I}\begin{cases} u_I = \sum_{n=1}^{\infty} \frac{r^{\frac{n}{2}}}{2\mu} a_n \left\{ \left[ \kappa + \frac{n}{2} + (-1)^n \right] \cos\frac{n\theta}{2} - \frac{n}{2}\cos\frac{(n-4)\theta}{2} \right\} \\ v_I = \sum_{n=1}^{\infty} \frac{r^{\frac{n}{2}}}{2\mu} a_n \left\{ \left[ \kappa - \frac{n}{2} - (-1)^n \right] \sin\frac{n\theta}{2} + \frac{n}{2}\sin\frac{(n-4)\theta}{2} \right\} \end{cases} \quad (1)$$

and,

$$\text{Mode II}\begin{cases} u_{II} = -\sum_{n=1}^{\infty} \frac{r^{\frac{n}{2}}}{2\mu} b_n \left\{ \left[ \kappa + \frac{n}{2} - (-1)^n \right] \sin\frac{n\theta}{2} - \frac{n}{2}\cos\frac{(n-4)\theta}{2} \right\} \\ v_{II} = \sum_{n=1}^{\infty} \frac{r^{\frac{n}{2}}}{2\mu} b_n \left\{ \left[ \kappa - \frac{n}{2} + (-1)^n \right] \cos\frac{n\theta}{2} + \frac{n}{2}\cos\frac{(n-4)\theta}{2} \right\} \end{cases} \quad (2)$$

where, $u$ and $v$ are horizontal (x direction) and vertical (y direction) displacements in mode *I* and *II*. $\mu$ is the shear modulus and $\kappa = (3-\nu)/(1+\nu)$ for plane stress and $\kappa = 3-4\nu$ for plane strain conditions, where $\nu$ is the Poisson's ratio. $a$ and $b$ are constants and $r$ and $\theta$ are radial and phase distance from crack tip.

Mixed mode displacement fields ($u$ and $v$) which are obtained from DIC, can be derived by superimposing the mode I and II displacement fields. By defining $f_{n,m}(r,\theta)$, $g_{n,m}(r,\theta)$, $h_{n,m}(r,\theta)$ and $l_{n,m}(r,\theta)$ as follows (equation 3); the displacement field (equations 1 and 2) can be written in a matrix form (equation 4).

$$
\begin{aligned}
f_{n,m} &= \frac{r_m^{\frac{n}{2}}}{2\mu}\left\{\left[\kappa+\frac{n}{2}+(-1)^n\right]\cos\frac{n\theta_m}{2}-\frac{n}{2}\cos\frac{(n-4\theta_m)}{2}\right\} \\
g_{n,m} &= \frac{-r_m^{\frac{n}{2}}}{2\mu}\left\{\left[\kappa+\frac{n}{2}-(-1)^n\right]\sin\frac{n\theta_m}{2}-\frac{n}{2}\sin\frac{(n-4\theta_m)}{2}\right\} \\
h_{n,m} &= \frac{r_m^{\frac{n}{2}}}{2\mu}\left\{\left[\kappa-\frac{n}{2}-(-1)^n\right]\sin\frac{n\theta_m}{2}+\frac{n}{2}\sin\frac{(n-4\theta_m)}{2}\right\} \\
l_{n,m} &= \frac{r_m^{\frac{n}{2}}}{2\mu}\left\{\left[\kappa-\frac{n}{2}+(-1)^n\right]\cos\frac{n\theta_m}{2}+\frac{n}{2}\cos\frac{(n-4\theta_m)}{2}\right\}
\end{aligned}
\tag{3}
$$

$$
\begin{Bmatrix} u_1 \\ \vdots \\ u_m \\ v_1 \\ \vdots \\ v_m \end{Bmatrix} = \begin{bmatrix} f_{1,1}\cdots f_{n,1} & g_{1,1}\cdots g_{n,1} \\ \vdots & \vdots \\ f_{1,m}\cdots f_{n,m} & g_{1,m}\cdots g_{n,m} \\ h_{1,1}\cdots h_{n,1} & l_{1,1}\cdots l_{n,1} \\ \vdots & \vdots \\ h_{1,1}\cdots h_{n,1} & l_{1,1}\cdots l_{n,1} \end{bmatrix} \begin{Bmatrix} a_1 \\ \vdots \\ a_n \\ b_1 \\ \vdots \\ b_n \end{Bmatrix} \tag{4}
$$

where *m* is the data point index.

By expanding equations 1 and 2, keeping the terms up to order $r^{3/2}$ and comparing with the more common notation, i.e. using stress intensity factors and T-stress, it can be shown that

$$
K_I = a_1\sqrt{2\pi}\ ,\ K_{II} = -b_1\sqrt{2\pi}\ ,\ T = 4a_2 \tag{5}
$$

in which $K_I$ is the mode I stress intensity factor, $K_{II}$ is mode II stress intensity factor and $T$ is the T-stress.

Looking at equation 4 it is evident that no rigid body motion term has been considered in that equation. This can be compensated for by adding constant terms in equation 4 to compensate for the rigid body translations and another term to compensate for the rigid body rotation as follows,

$$\begin{Bmatrix} u_1 \\ \vdots \\ u_m \\ v_1 \\ \vdots \\ v_m \end{Bmatrix} = \begin{bmatrix} 1 & f_{1,1} \cdots f_{n,1} & 0 & g_{1,1} \cdots g_{n,1} & -r_1 \sin\theta_1 \\ \vdots & \vdots & \vdots & \vdots & \vdots \\ 1 & f_{1,m} \cdots f_{n,m} & 0 & g_{1,m} \cdots g_{n,m} & -r_m \sin\theta_m \\ 0 & h_{1,1} \cdots h_{n,1} & 1 & l_{1,1} \cdots l_{n,1} & r_1 \sin\theta_1 \\ \vdots & \vdots & \vdots & \vdots & \vdots \\ 0 & h_{1,1} \cdots h_{n,1} & 1 & l_{1,1} \cdots l_{n,1} & r_m \cos\theta_m \end{bmatrix} \begin{Bmatrix} a_0 \\ a_1 \\ \vdots \\ a_n \\ b_0 \\ b_1 \\ \vdots \\ b_n \\ R \end{Bmatrix} \quad (6)$$

where $a_o$ and $b_o$ are used to compensate for the rigid body motion and $R$ compensates for the rigid body rotation.

***Experimental results and discussion***

Experiments were undertaken on both sharp notches and fatigue cracks emanating from notches in specimens manufactured from 7010 T7651 aluminium alloy. Pure mode I loading condition was created ahead of a 4mm notch in a 5mm thick DCB specimen with the dimensions shown in Figure 1.

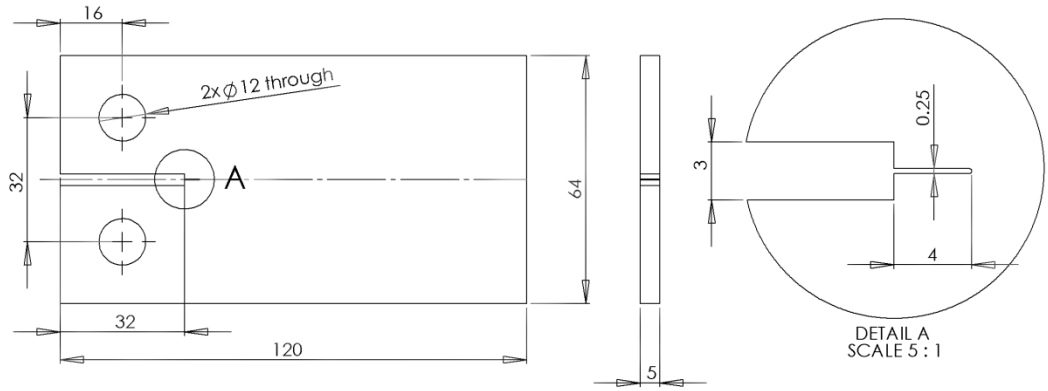


Figure 1: DCB specimen dimensions in mm

The specimen was machined from a plate of 7010 T7651 aluminium alloy and spark eroded to introduce the notch into the specimen. The required speckles for DIC were produced on the surface of specimen using a fine spray of matt black paint. A 100kN MAND hydraulic test machine was used to load the specimen. A load range of 0.5kN to 1.5kN was applied to the specimen. A 14 bit, 1600x1200 CCD camera and a Nikon lens with a resolution of 18.75 microns per pixel was used to record the images. DaVis software

[11] was employed to correlate the images. Figure 2 shows a typical correlated displacement field obtained around a crack. The experiments were continued by growing a fatigue crack from the notch tip, using a 0.5kN to 2kN load range at a loading frequency of 15Hz. The crack growth was paused when the fatigue crack length was approximately 1mm, 4mm, 8mm and 15mm. For each increment of crack growth load ranges of 0.5kN to 1.5kN was applied, images were recorded at each load and processed to determine the stress intensity factors and T-stress.

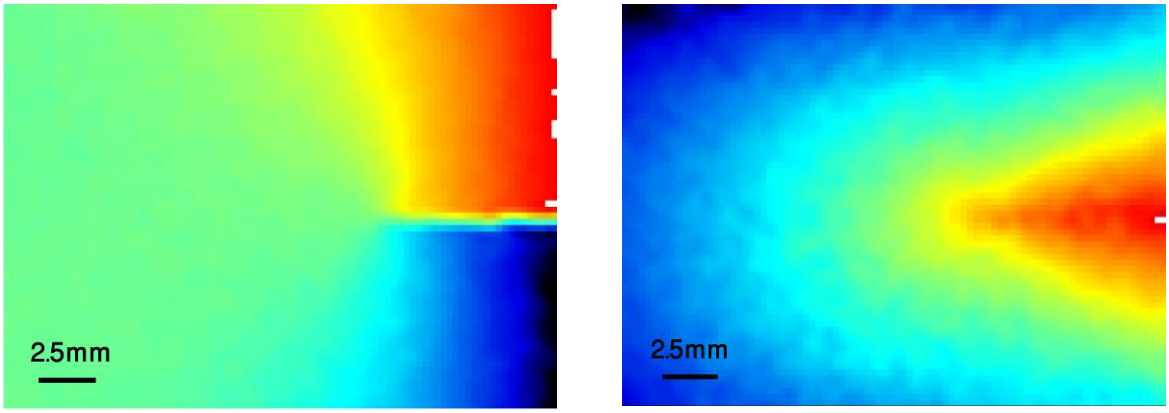


Vertical displacement Horizontal displacement

Figure 2: Typical correlated displacement fields obtained around a crack using DIC

The displacement field obtained from DIC was imported to the DICITAC software [5] to determine the stress intensity factors and the T-stress using equations 5 and 6 under plane stress conditions. In the solution process of equation 6, the number of terms was increased until the stress intensity factors and the T-stress converged as typically shown in Figure 3 for the 8mm fatigue crack example. These figures also show the quality of the fitted data to the experimental displacement fields. The fitted data shown in Figure 3 (a) and (b) are based on the recreation of the displacement fields using the coefficients of 15 terms of Williams' solution.

a)

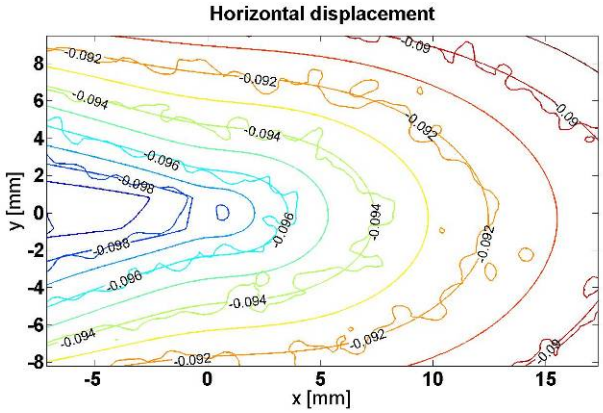


b)

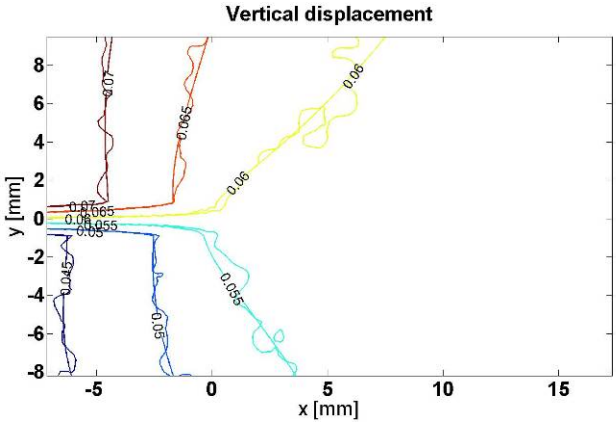


c)

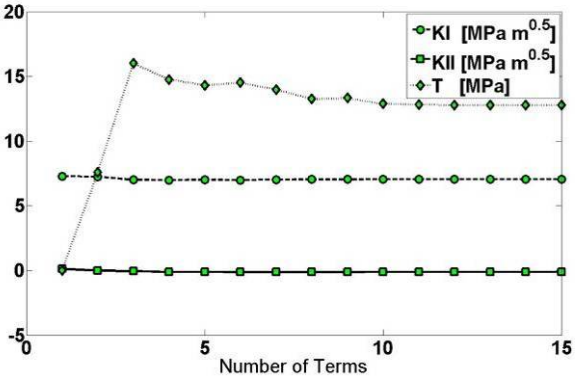


Figure 3: Quality of fitted displacement field a) horizontal and b) vertical and c) variation of T-stress and SIF versus number of Williams' solution terms for the 8mm fatigue crack under 0.5 to 1.5 kN loading condition

In parallel with the experiments, the finite element method, ABAQUS/CAE, was used to find the stress intensity factors and T-stress. In order to check the accuracy of the numerical analysis, a uniaxial tensile model was generated for a centre-cracked large plate with $a/w$=0.08 and $w/h$=1, in which $a$ is the crack length, $w$ is width of specimen and $h$ is height of specimen. The T-stress was determined for a range of loads and compared to an analysis published by Fett [12]. The results showed only 0.6% difference when compared to the published data. A double-edge-cracked rectangular plate ($a/w$=0.4 and $h/w$>1.5) was also modelled using FE. In this case T-stress results were about 2% different from those in reference [12]. Therefore it was considered that the FE method could be used as a comparison for the experiments.

In numerical simulation of the problem, an elastic model as shown in Figure 4 was used in ABAQUS. Quarter point singular elements used to model the elastic singularity ahead of the crack tip and the stress intensity factors were determined using the J integral method. The T-stress was also determined using an interaction integral technique.

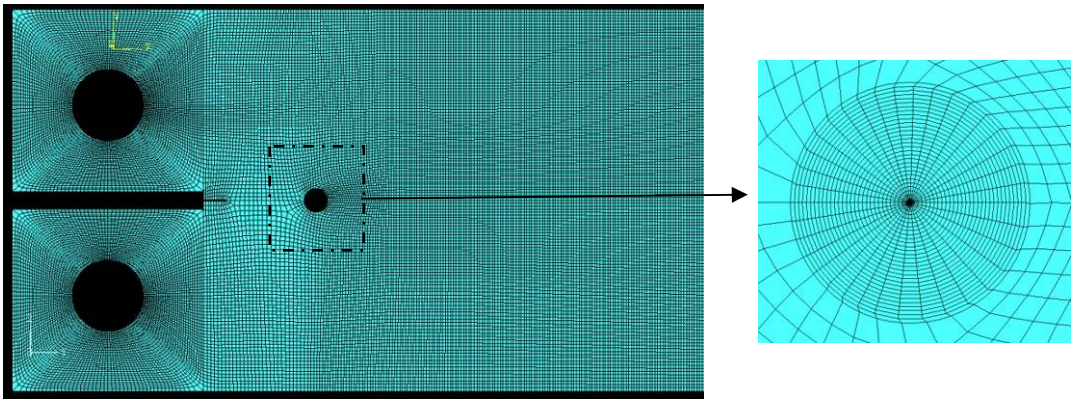

Figure 4: FE model created in ABAQUS

Experimentally determined mode I stress intensity factors are in good agreement with the numerically simulated cases, see Figure 5(a). The average differences were 12.6% (with standard deviation of 8.8%) using 3 terms solution and 12.9% (with standard deviation of 11.5%) using converged term solution.

Almost the same trend as the mode I stress intensity factors is observed (Figure 5 (b)) for the experimentally determined T-stress when compared to the FE results. The average differences of 24.9% (with standard deviation of 2.2%) and 35.4% (with standard deviation of 14.9%) were found using 3 terms and converged term solutions, respectively. The agreement between the numerical and experimental results obtained for the T-stress is not

as good as for the stress intensity factor results. Compared to the stress intensity factor, the T-stress is one order higher and this makes the T-stress relatively a more difficult parameter to measure experimentally. Nevertheless, some of the discrepancy is likely to be due to the limitations of the finite element model. The realities of a non-planar crack, crack front curvature, surface residual stresses from machining and material anisotropy will all compromise the modelling. Given the consistency and smooth trend in the experimental T stress values, the proposed methodology provides a reliable and robust technique for determining elastic constraint in fatigue and fracture testing.

a)

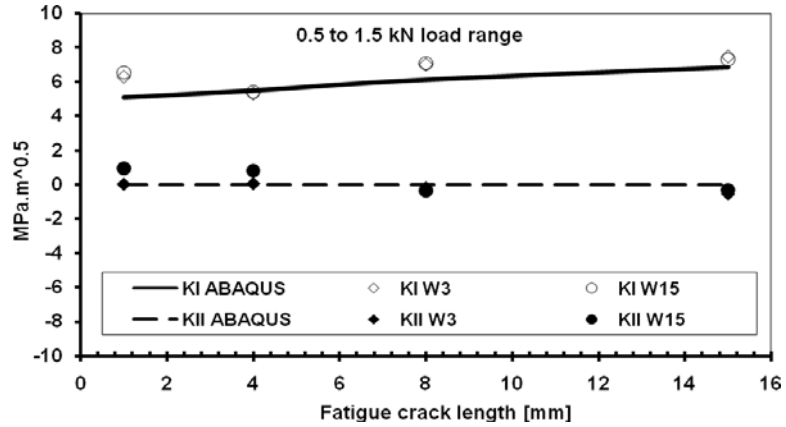


b)

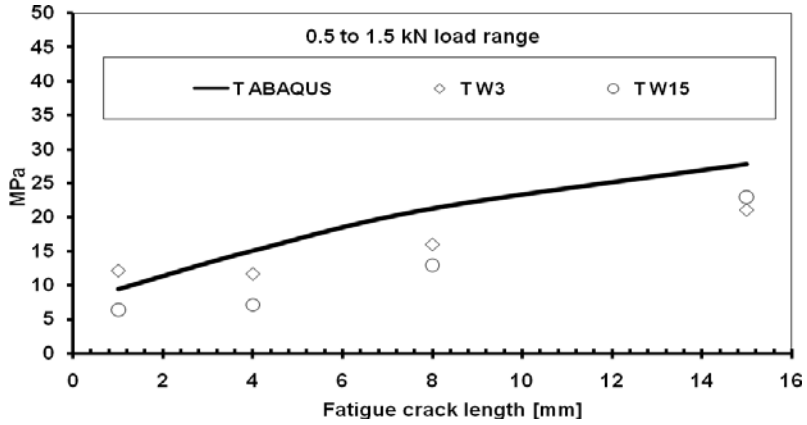


Figure 5: Comparison of a) stress intensity factors and b) T-stresses determined using ABAQUS, 3 terms Williams (W3) and 15 terms Williams (W15) for 0.5 to 1.5 kN load range

## DETERMINING CTOA IN THE PRESENCE OF EXTENSIVE PLASTICITY

### *CTOA fracture criterion*

The CTOA fracture criterion is an evolution of the well established crack tip opening displacement (CTOD) criterion. The basic hypothesis is that for a given alloy with sufficiently large tearing modulus and a degree of hardening, there is a clearly definable crack tip profile and CTOA [13]. The constant CTOA value obtained in the stable phase of crack extension can be used in numerical methods to predict the fracture behaviour of a structure made from the same alloy. Figure 6 illustrates the definition of CTOA and CTOD.

The constant CTOA value ($CTOA_{material}$) is considered to be the material fracture resistance and if the crack driving force, measured by the $CTOA_{applied}$ of the loaded structure, causes the inequality (1) to be fulfilled, the fracture process will be arrested. However, the fracture process will continue if the inequality is reversed.

$$CTOA_{material} > CTOA_{applied}$$

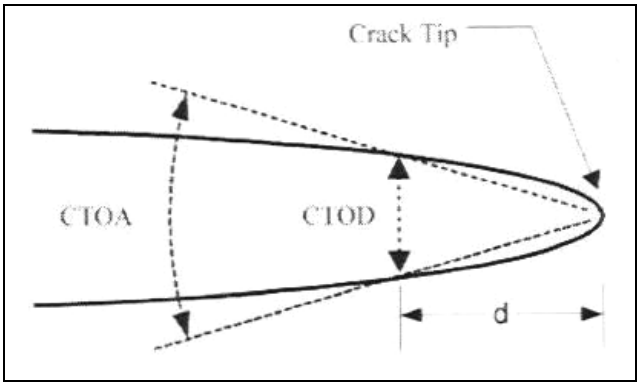


Figure 6: Definition of CTOA and CTOD

### *Methodology*

In this work, experiments to determine CTOA from displacement fields was carried out using an aerospace grade aluminium alloy. The geometry of the compact tension (CT) specimen used adhered to the guidelines set in the ASTM E2472 standard [14] which is designed for fracture toughness data under low through thickness constraint conditions. In this case, the low constraint conditions were satisfied by the plate thickness which was 5.0 mm and the resultant geometry of the specimen is illustrated in Figure 7. The geometry of

the CT specimen gave an initial crack length to width ratio of approximately 0.4 after fatigue pre-cracking which was carried out to obtain a sharp initial crack tip.

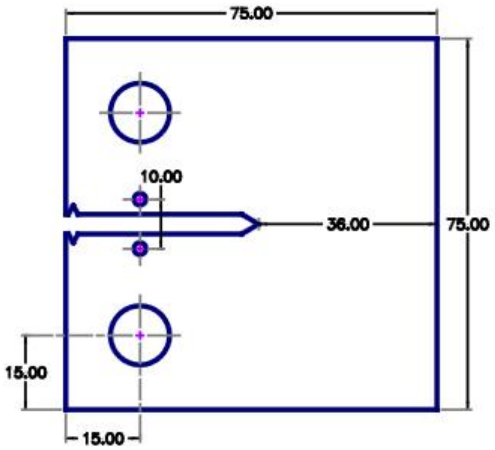


Figure 7: Schematic of CT specimen

To facilitate the use of DIC to obtain displacement field measurements, a random speckle was applied to the surface of the specimen in a 10 mm thick strip along the entire mid-section of the specimen as shown in Figure 8. A grid (1.0 × 2.0 mm) was etched onto the surface before the speckle pattern was applied and was used predominantly for crack tracking purposes. The specimens were fractured under mode I conditions in a 100 kN servo hydraulic machine. Loading grips were designed to minimise buckling and twisting of the specimens. The test was conducted under quasi-static conditions in displacement control at a rate of 0.02 mm/s. Data acquisition was done using the integrated DIC system which allowed all the test parameters to be synchronised.

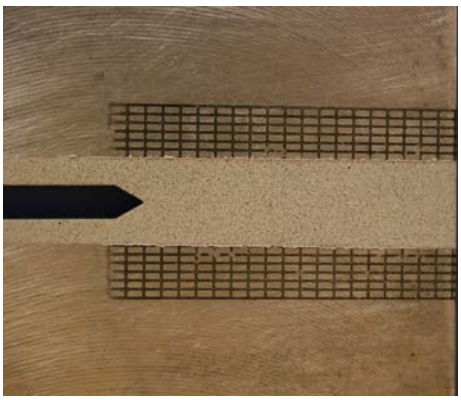

Figure 8: Prepared specimen with speckle pattern and grid (1.0 × 2.0 mm) on the surface

CTOA was calculated from displacement fields measured using DIC as shown in Figure 9. Two points, one above the crack tip and one below the crack tip along the same vertical axis, are chosen from which the relative vertical displacement is calculated. The distance to the crack tip is calculated from the coordinates from which CTOA is derived from equation 7 below.

$$CTOA_{\theta} = 2\tan^{-1}\frac{(V_b - V_a)}{2A} \tag{7}$$

Where, $A$ = distance from crack tip to measurement position

$V_b$ = vertical vector displacement below crack tip

$V_a$ = vertical vector displacement above crack tip

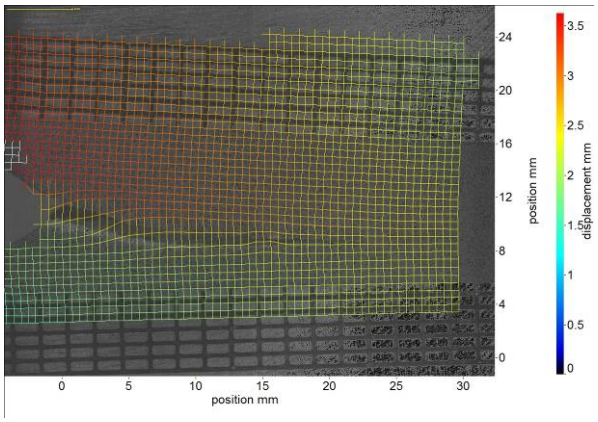


Figure 9: Displacement fields measured with DIC

***Results***

Displacement fields measured for one particular specimen at different stages of crack extension is shown in Figure 10. The origin of the X and Y coordinates correspond to the location of the crack tip and the XY plane represents the planar surface of the specimen. Values of the vertical displacement are absolute values with rigid body displacements subtracted. There are minimal differences in the displacement field data around the crack tip between the different crack lengths which suggest that there are only small differences in the respective crack geometries. The displacement field data also shows that there is significant plastic deformation around the crack path which is evident from the reduction in the measured displacement values.

a)

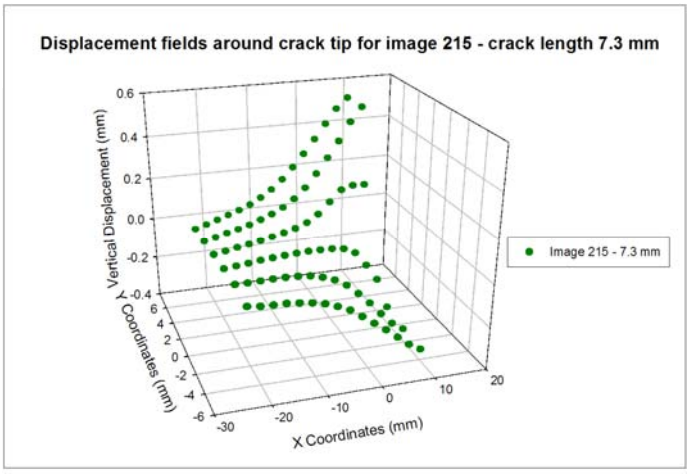


b)

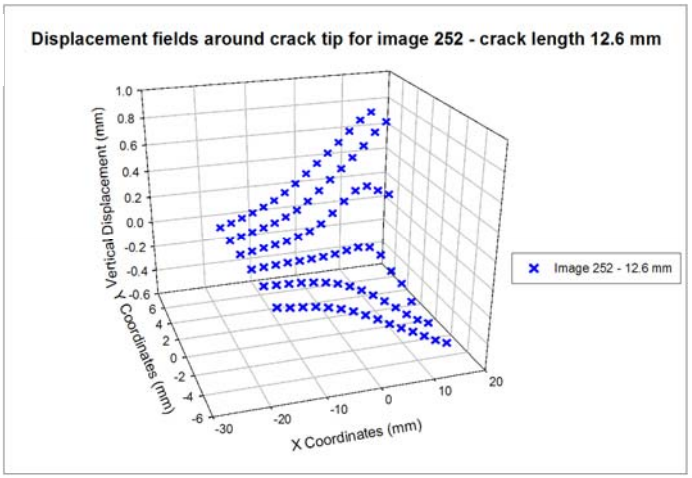


Figure 10: Displacement fields for different crack lengths

From the displacement field data, CTOA values were computed from the corresponding data points using the CTOA calculation methodology explained in the preceding section. The CTOA distribution obtained is shown in Figure 11. The star symbol in the plot pinpoints the location of the crack tip and the coordinate system in the XY direction is identical to the plots in Figure 10. From the two CTOA distribution graphs, it is clear that the ahead of the crack tip, there is a rapid decrease in CTOA values. At a distance of approximately 7.5 mm ahead of the crack tip, the net displacements measured were negligible and the corresponding CTOA values clearly show this.

Behind the crack tip, the resultant CTOA values clearly indicate that there is a measurable angle which remains relatively unchanged until the corresponding data points approaches the crack tip where an increase in CTOA values is observed. This increase is

normally observed when the distance between the two corresponding points in the Y-direction is bigger than the distance of the crack tip to corresponding measurement points in the X-direction. Further discussion on this effect can be found in literature [15]. Figure 12 shows all the data points in Figure 11 plotted in 2D which further emphasises the observation. The legend labels ‘a’ and ‘b’ denote the respective crack lengths of 7.3 mm and 12.6 mm. The numbers in the data labels are the Y coordinates of the vector location on the specimen surface and the crack tip location is at the origin of the X-axis. The average CTOA value obtained in the 5 – 20 mm region behind the crack tip was 6.23° which corresponded very well to the values obtained using other more conventional techniques ($d_5$ and ASTM DIC method [14]) used to measure CTOA for this particular specimen.

a)

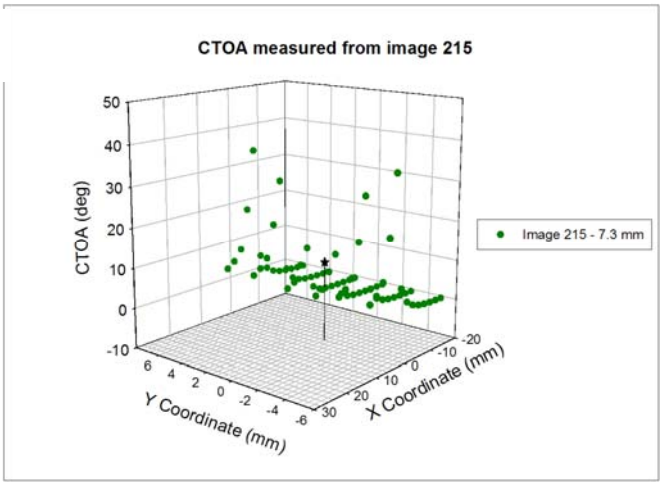


b)

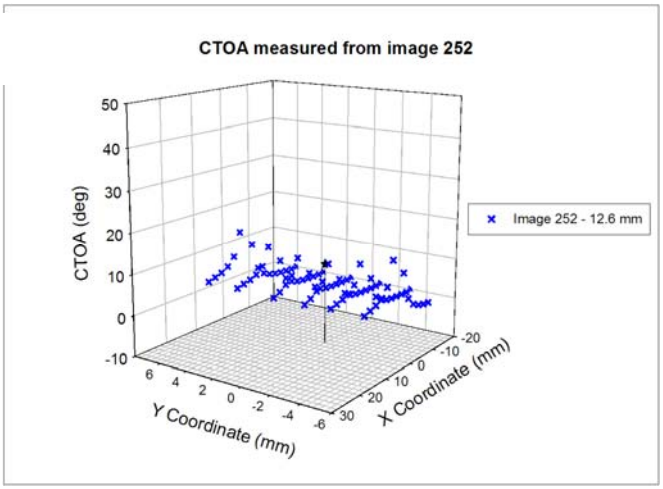


Figure 11: CTOA distribution derived from displacement fields. The star location identifies the crack tip location

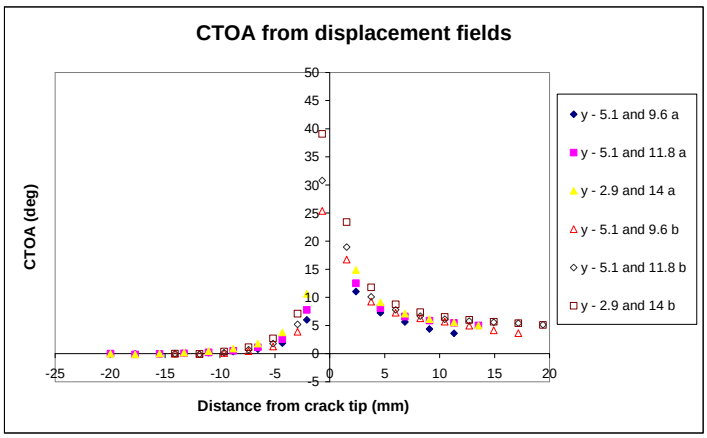


Figure 12: 2D plot of CTOA values shown in Figure 11

Results from the calculation of CTOA from displacement field measurements have shown that it is possible to obtain consistent CTOA data from full field displacement data measured using DIC. However, adequate measures need to be taken to discriminate data affected by extensive plasticity close to the crack path and the measurement length effect discussed earlier. The accuracy and consistency of the CTOA obtained from the DIC measured displacements and extraction of data has allowed for CTOA to be used as a realistic measure of tearing toughness. Figure 13 demonstrates the capability of the technique to be able to discriminate the change in tearing toughness caused by material anisotropy which in this particular case was significant.

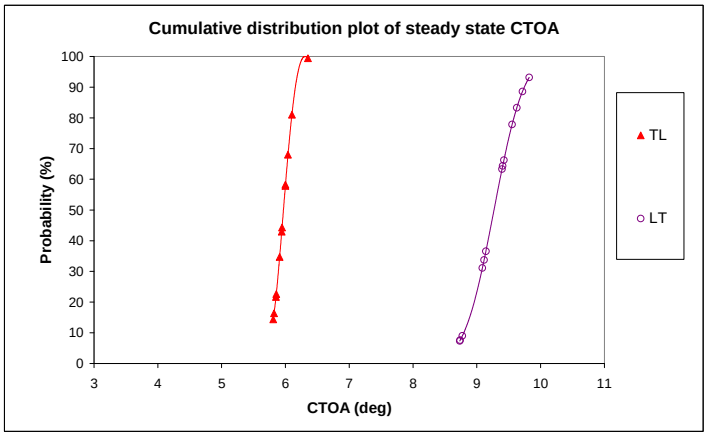


Figure 13: Cumulative distribution plot of CTOA values illustrating anisotropy

## CONCLUDING DISCUSSION

Direct measurement of the crack tip displacement field under both cyclic and monotonic loading is now readily performed using digital image correlation of pairs of images taken of a cracked structure. Most usefully, the displacement data contains both elastic and plastic contributions.

Analysis of the full field data for a cyclically loaded crack can provide the T-stress term of the Williams' stress field expansion. This provides valuable experimental information on the effect of geometry on the crack tip constraint and hence the path stability of growing cracks.

The ability to capture extensive non-linear crack tip displacements has opened up the possibility of using the crack tip opening angle as a realistic design and assessment parameter for stable ductile tearing. The accurate and extensive data that is now available enables subtle differences in tearing behaviour to be determined. The role of anisotropy and metallurgical processing on ductile tearing can now be investigated in a systematic manner.

## REFERENCES


1. Patterson, E.A. and Olden, E.J., (2004) Fatigue and Fracture of Engineering Materials and Structures. (27(7)): p. 623 - 636.
2. P. López-Crespo, A. Shterenlikht, E. A. Patterson, J. R. Yates, and P. J. Withers. in *Proceedings of the Society for Experimental Mechanics Annual Conference and Exposition*. 2006. St Louis, Missouri, USA.
3. Yoneyama S, Morimoto Y, and Takashi M, (2006) Strain. **42** (1): p. 21 - 29.
4. Hild F and Roux S, (2006) C. R. Mecanique. **334** (1): p. 8 - 12.
5. Zanganeh Gheshlaghi M,(2008). PhD, Dept of Mechanical Engineering, The University of Sheffield.
6. Abanto-Bueno J and Lambros J, (2005) International Journal of Solids and Structures. **43** (13): p. 3920-3939.
7. Newman J C Jr, James M A, and Zerbst U, (2003) Engineering Fracture Mechanics. **70** (3-4): p. 371 - 385.
8. Newman J C Jr and Schwalbe K-H. in *11th International Conference on Fracture*. 2005. Turin, Italy. 6.
9. Muskhelishvili N I, *Some Basic Problems of the Mathematical Theory of Elasticity*. 4th ed. 1977, Leyden, The Netherlands: Noordhoff International.

10. Williams M L, (1957) Journal of Appllied Mechanics. (27): p. 109-114.

11. LA Vision, *Davis StrainMaster Software for Davis 7.0*. 2005. 386.

12. Fett T, (1998) Engineering Fracture Mechanics. **60** (5-6): p. 631-652.

13. Barnby J T, Nadkarni A S, and Cresswell S L, (1995) International Journal of Materials and Product Technology. **10** (1): p. 161-170.

14. ASTM-E2472 (2006),*Standard Test Method for Determination of Resistance to Stable Crack Extension under Low-Constraint Conditions*,

15. Tai Y H,(2008). PhD, Dept of Mechanical Engineering, University of Sheffield.